High Resolution Spectroscopy of HCN Isotopomers: $H^{13}CN$, $HC^{15}N$, and $H^{13}C^{15}N$ in the Ground and First Excited Bending Vibrational State

U. Fuchs, S. Brünken, G. W. Fuchs, S. Thorwirth[a], V. Ahrens, F. Lewen, Š. Urban[b], T. Giesen, and G. Winnewisser

I. Physikalisches Institut, Universität zu Köln, Zülpicher Str. 77, 50937 Köln, Germany
[a] *Present address:* Department of Engineering and Applied Sciences Harvard University, 29 Pierce Hall, Cambridge, MA 02138 and Harvard-Smithsonian Center for Astrophysics, U. S. A.
[b] Institute of Chemical Technology, Department of Analytical Chemistry, Technická 5, 166 28 Prague 6, Czech Republic and Academy of Sciences of the Czech Republic, J. Heyrovský Institute, of Physical Chemistry, Dolejskova 3, 182 23 Praha 8, Czech Republic

Reprint requests to Dr. T. G.; E-mail: giesen@ph1.uni-koeln.de, Fax: +49 221 470 5162

Z. Naturforsch. **59a,** 861 – 872 (2004); received August 20, 2004

The eleven energetically lowest pure rotational transitions, $J \leftarrow J-1$ ($J = 1, 2, \ldots, 11$), of $H^{13}CN$, $H^{13}C^{15}N$, and $HC^{15}N$ in the ground and first excited bending state were measured. By operating the Cologne Tetrahertz Wave Spectrometer up to 1 THz in the sub-Doppler mode, a transition frequency accuracy of a few kHz is achieved. These measurements were carried out at frequencies between 80 – 950 GHz. In addition, some transitions of the three isotopomers with rotational quantum numbers $J = 20, 21, 22, 23$ have been measured in Doppler-limited resolution near 2 THz, using the frequency stabilized Cologne Sideband Spectrometer for Terahertz Applications (COSSTA). Furthermore, direct *l*-type transitions of $H^{13}CN$ in the first excited bending state with J up to 35 have been measured. These new data are of particular importance, since we discovered highly excited circumstellar $H^{12}CN$ recently. A global fit of the newly enlarged data set together with existing carefully screened ro-vibrational data yields molecular constants which are highly reliable and of great importance both for astrophysical observations and laboratory applications.

Key words: Molecular Spectroscopy; Sub-Doppler Spectroscopy; High Resolution Spectroscopy; HCN; Microwave Spectroscopy; THz Spectroscopy; Hyperfine Structure; Direct *l*-type Transition.

1. Introduction

Recently, our laboratory has undertaken on HCN a combined laboratory and interstellar investigation. The results have been partly published in the form of six papers on HCN [1 – 5] and DCN [6]. From the five papers on HCN, [2, 3] rely essentially on saturation dip measurements, which can routinely be carried out with our Cologne Terahertz Spectrometer up to about 1 THz. Paper [4] presents precise measurements of $H^{12}CN$ and $H^{13}CN$ ground state pure rotational lines from 265 GHz up to 1.6 THz, which were obtained by employing the techniques of planar Schottky diode multipliers pumped by **B**ackward **W**ave **O**scillators (BWOs). The paper [5] consists of a collaboration with our colleagues from Prof. T. Amano's group at Ibaraki University and concentrates on the higher excited vibrational states, which are measured exclusively in Doppler limited resolution.

The present paper contains our recent sub-Doppler laboratory data on $H^{13}CN$, $H^{13}C^{15}N$ and $HC^{15}N$ in the ground and first excited bending state.

The most comprehensive work to date on the pure rotational spectra of these species is by Preusser and Maki [7], who recorded low J rotational transitions between 170 and 450 GHz for the ground and several vibrational excited states. The hyperfine structure of $H^{13}CN$ was, however, not fully resolved by their Doppler-limited measurements. The same holds for transitions reported in our previous paper [4] on HCN and $H^{13}CN$. Additional information on the hyperfine structure of $H^{13}CN$ can be found in [8] by Pearson *et al.*, who investigated the $J = 1 \leftarrow 0$ and $J = 2 \leftarrow 1$ transitions of all three isotopomers in the vibrational ground state. Therefore, to constrain the molecular

hyperfine constants for $H^{13}CN$ and higher order centrifugal distortion parameters for all isotopomers, we performed high accuracy sub-Doppler (up to 1 THz) and Doppler measurements (around 2 THz) in both the vibrational ground and first excited bending state.

This present paper is also in response to our recent investigation of new, highly excited states including direct *l*-type transitions of $H^{12}CN$ in the $\upsilon_2 = 1$ state [3]. These laboratory data were supplemented by using the full sensitivity of the 100 m telescope of the Max Planck Institute for Radioastronomy at Effelsberg to detect the *l*-type doubling transitions of HCN in the hot circumstellar envelope CRL 618 (Thorwirth et al., 2003 [1]).

In a similar approach, we measured direct *l*-type transitions of $H^{13}CN$ to high *J*-values and frequency, extending the range of known transitions (as reported by Winnewisser et al. [9]) considerably.

All these measurements are to be seen within the framework of a broad contribution from the laboratory of the *Cologne Observatory for sub-Millimeter Astronomy*, KOSMA, in providing highly precise state of the art data sets on molecules of astrophysical importance, e.g., CO, CS, and free radicals with their isotopomers. These data will be published in the CDMS (Cologne Database for Molecular Spectroscopy) as a service to the astronomical community interested primarily in molecular line work (See the web site www.cdms.de) [10].

The remainder of this paper on the HCN isotopomers will follow the lines chosen for the $H^{12}CN$ isotopomer paper [2]. We will refer quite extensively to this paper because we used it to pave the way which all other papers in this series follow. After a short description of the configurations of the spectrometers employed, we will give a quick overlook of the measurements and the analysis of the data as well as a discussion of the degree of reliance of additional transition frequency predictions.

2. Experimental Techniques

In principle, with our spectrometers, we are able to cover a broad frequency region from about 54 GHz (microwave region) to 2 THz, which corresponds to the shorter millimeter wave region. These spectrometers have been optimized for performance in three different frequency regions by using exclusively russian made BWOs as microwave power sources:

(i) At about 54 GHz to 178 GHz, where the direct *l*-type transitions of HCN reach their maximum intensity, we use a commercial spectrometer from Analytik & Messtechnik GmbH, Chemnitz (AMC) [11] to perform measurements with Doppler resolution.

(ii) The frequency region from about 70 GHz to 1 THz is basically reachable with the Cologne Terahertz Spectrometer, which has been described repeatedly in different journals (e. g. G. Winnewisser (1995) [12]). Due to the high output power of the employed BWOs and their high spectral purity, it is possible to use the spectrometer in sub-Doppler mode. To reach frequencies above 1 THz, the Cologne Terahertz spectrometer can be combined with different high frequency multipliers [4] at the output stages of the BWOs. These planar Schottky diode devices have been used in the KOSMA laboratories of Cologne University to cover the frequency region between 1 and 2 THz.

(iii) The third spectrometer is the **Co**logne **S**ideband **S**pectrometer for **T**Hz **A**pplications (COSSTA), which has been optimized to operate at present from 1.75 to 2.01 THz [13, 14]. The use of different gases in the pump laser allows, in principle, wide tuning steps to be taken. The uniqueness of this spectrometer rests in the mixing of the frequency-stabilized radiation of a FIR ring-laser system operated at a fixed frequency system of 1.626 THz with the output of a frequency- and phase-stabilized BWO.

3. Measurements

All measurements performed on the different isotopomers of HCN were carried out with isotopically enriched samples. The pressure in the absorption cell was kept at a dynamical pressure level between $8 \cdot 10^{-3}$ and 0.15 Pa for the sub-Doppler measurements. However, the Doppler limited measurements on high *J* R-branch and on the direct *l*-type transitions require 0.1 to 1 Pa at temperatures of 300 and 500 K. For each of the three isotopomers $H^{13}CN$, $HC^{15}N$, and $H^{13}C^{15}N$, the energetically lowest rotational transitions $J \leftarrow J-1$ in the ground ($J = 1, 2, \ldots, 11$) and first excited bending state ($J = 2, 3, \ldots, 11$) were measured. In addition we observed some high *J* transitions up to $J = 24 \leftarrow 23$ in the 2 THz range and, for $H^{13}CN$, direct *l*-type transitions for *J* up to 35.

The data presented here on $H^{13}CN$ are unique in the sense that all the rotational transition frequencies up to 1 THz have been recorded by saturation tech-

Table 1. Hyperfine transitions and crossover dips of $H^{13}CN$ in the ground vibrational state. For each transition the corresponding standard deviation (σ), a difference *obs.* – *calc.*, calculated relative (^{R}I) and absolute (^{A}I) intensities are given (except for the highest frequencies). The absolute intensities are the dimensionless intrinsic line strengths. Both intensities are listed for the linear as well as saturation experiment. In the case where the two crossover transitions originating from either a common upper or lower energy level overlap, only the entry for the common lower level is given. The intensities of both transitions vary in the range of a few percent only.

J'	F'	←	J''	F''	ν (σ) / MHz	Diff. / MHz	$^{A}I_{\rm lin}$	$^{R}I_{\rm lin}$	$^{A}I_{\rm sat}$	$^{R}I_{\rm sat}$
1		←	0		86339.9181(0003)					
1	1	←	0	1	86338.733(005)	−0.001	1.00E+00	33.33	1.00E+00	25.71
1	2	←	0	1	86340.163(005)	−0.002	1.67E+00	55.56	2.78E+00	71.43
1	0	←	0	1	86342.251(005)	−0.004	3.33E−01	11.11	1.11E−01	2.86
2		←	1		172677.8445(0005)					
2	2	←	1	2	172676.414(005)	−0.004	5.00E−01	8.33	2.50E−01	2.27
2	1	←	1	0	172676.665(005)	0.002	6.67E−01	11.11	4.44E−01	4.03
2	2	←	1	1	172677.845(005)	−0.004	1.50E+00	25.00	2.25E+00	20.39
2	3	←	1	2	172677.956(005)	−0.004	2.80E+00	46.67	7.84E+00	71.04
2	1	←	1	1	172680.182(005)	−0.002	5.00E−01	8.33	2.50E−01	2.27
3		←	2		259011.7877(0008)					
3	3	←	2	3	259010.255(005)	0.002	3.33E−01	3.70	1.11E−01	0.44
3	2	←	2	1	259011.543(005)	−0.007	1.80E+00	20.00	3.24E+00	12.72
3	3	←	2	2	259011.798(005)	0.003	2.67E+00	29.63	7.11E+00	27.92
3	4	←	2	3	259011.866(005)	0.006	3.86E+00	42.86	1.49E+01	58.42
3	2	←	2	2	259013.884(005)	0.000	3.33E−01	3.70	1.11E−01	0.44
4		←	3		345339.7561(0012)					
4	4	←	3	4	345338.165(005)	0.006	2.50E−01	2.08	6.25E−02	0.14
4	3	←	3	2	345339.644(010)	−0.011	2.86E+00	23.81	8.16E+00	17.64
4	4	←	3	3	345339.788(010)	0.022	3.75E+00	31.25	1.41E+01	30.39
4	5	←	3	4	345339.788(010)	−0.023	4.89E+00	40.74	2.39E+01	51.65
4	3	←	3	3	345341.749(005)	0.004	2.50E−01	2.08	6.25E−02	0.14
4	4/5	←	3	4/4	345338.980(005)	−0.005			2.60E−03	0.01
5		←	4		431659.7586(0016)					
5	5	←	4	5	431658.122(005)	0.004	2.00E−01	1.33	4.00E−02	0.05
5	4	←	4	3	431659.701(005)	−0.004	3.89E+00	25.93	1.51E+01	20.65
5	5	←	4	4	431659.791(010)	0.021	4.80E+00	32.00	2.30E+01	31.46
5	6	←	4	5	431659.791(010)	−0.014	5.91E+00	39.39	3.49E+01	47.69
5	4	←	4	4	431661.683(005)	−0.001	2.00E−01	1.33	4.00E−02	0.05
5	5/6	←	4	5/5	431658.954(005)	−0.007			1.95E−02	0.03
5	4/5	←	4	4/4	431660.726(010)	−0.001			4.89E−03	0.01
6		←	5		517969.8039(0021)					
6	5	←	5	4	517969.821(010)	0.048	4.91E+00	27.27	2.41E+01	22.67
6	6	←	5	5	517969.821(010)	0.003	5.83E+00	32.41	3.40E+01	32.01
6	7	←	5	6	517969.821(010)	−0.025	6.92E+00	38.46	4.79E+01	45.09
6	5	←	5	5	517971.682(010)	−0.005	1.67E−01	0.93	2.78E−02	0.03
6	5/6	←	5	5/5	517970.752(010)	0.000			2.95E−02	0.03
6	6/7	←	5	6/6	517968.976(010)	−0.013			6.07E−02	0.06
7		←	6		604267.9013(0028)					
7	7	←	6	7	604266.207(005)	0.003	1.43E−01	0.68	2.04E−02	0.01
7	6	←	6	5	604267.914(010)	0.030	5.92E+00	28.21	3.51E+01	24.12
7	7	←	6	6	604267.914(010)	−0.004	6.86E+00	32.65	4.70E+01	32.32
7	8	←	6	7	604267.914(010)	−0.027	7.93E+00	37.78	6.29E+01	43.26
7	6	←	6	6	604269.754(005)	0.002	1.43E−01	0.68	2.04E−02	0.01
7	7/8	←	6	7/7	604267.071(005)	−0.002			1.23E−01	0.08
7	6/7	←	6	6/6	604268.834(005)	−0.001			8.24E−02	0.06
8		←	7		690552.0604(0036)					
8	8	←	7	8	690550.341(005)	−0.001	1.25E−01	0.52	1.56E−02	0.01
8	7	←	7	6	690552.079(010)	0.027	6.93E+00	28.89	4.81E+01	25.20
8	8	←	7	7	690552.079(010)	0.000	7.88E+00	32.81	6.20E+01	32.51
8	9	←	7	8	690552.079(010)	−0.021	8.94E+00	37.25	7.99E+01	41.91
8	7	←	7	7	690553.887(005)	0.001	1.25E−01	0.52	1.56E−02	0.01
8	8/9	←	7	8/8	690551.217(005)	−0.004			1.96E−01	0.10
8	7/8	←	7	7/7	690552.983(005)	0.000			1.57E−01	0.08
9		←	8		776820.2909(0045)					
9	8	←	8	7	776820.308(005)	0.019	7.94E+00	29.41	6.31E+01	26.06
9	9	←	8	8	776820.308(005)	−0.004	8.89E+00	32.92	7.90E+01	32.65
9	10	←	8	9	776820.308(005)	−0.023	9.95E+00	36.84	9.90E+01	40.88
9	8/9	←	8	8/8	776821.213(010)	0.009			2.40E−01	0.10
9	9/10	←	8	9/9	776819.431(010)	−0.012			2.71E−01	0.11
10		←	9		863070.634(005)	0.027				
11		←	10		949301.039(005)	0.023				
21		←	20		1810073.066(050)	0.010				
23		←	22		1981790.010(050)	−0.015				

Table 2. Hyperfine transitions and crossover dips of $H^{13}CN$ in the first excited bending vibrational state. For each transition the corresponding standard deviation (σ), a difference *obs.* – *calc*., calculated relative (^RI) and absolute (^AI) intensities are given (except for the highest frequencies). The absolute intensities are the dimensionless intrinsic line strengths. Both intensities are listed for the linear as well as saturation experiment. In the case where the two crossover transitions originating from either a common upper or lower energy level overlap, only the entry for the common lower level is given. The intensities of both transitions vary in the range of a few percent only.

J'	F'	←	J''	F''	υ_2	ν (σ) / MHz	Diff. / MHz	$^AI_{\rm lin}$	$^RI_{\rm lin}$	$^AI_{\rm sat}$	$^RI_{\rm sat}$
2		←	1		1^e	172627.3763(0005)					
2	2	←	1	1		172626.168(010)	−0.004	1.13E+00	25.00	1.27E+00	20.30
2	2	←	1	2		172626.931(005)	−0.001	3.75E−01	8.33	1.41E−01	2.26
2	1	←	1	1		172627.262(005)	0.003	3.75E−01	8.33	1.41E−01	2.26
2	3	←	1	2		172627.675(005)	0.003	2.10E+00	46.67	4.41E+00	70.72
2	1	←	1	0		172629.208(005)	−0.009	5.00E−01	11.11	2.50E−01	4.00
2		←	1		1^f	173486.6489(0005)					
2	2	←	1	1		173485.451(005)	0.006	1.13E+00	25.00	1.27E+00	20.30
2	2	←	1	2		173486.087(005)	−0.002	3.75E−01	8.33	1.41E−01	2.26
2	1	←	1	1		173486.716(005)	−0.008	3.75E−01	8.33	1.41E−01	2.26
2	3	←	1	2		173486.957(005)	0.004	2.10E+00	46.67	4.41E+00	70.72
2	1	←	1	0		173488.397(005)	0.004	5.00E−01	11.11	2.50E−01	4.00
3		←	2		1^e	258936.0518(0008)					
3	3	←	2	3		258935.008(005)	−0.001	2.96E−01	3.70	8.78E−02	0.44
3	3	←	2	2		258935.738(010)	−0.011	2.37E+00	29.63	5.62E+00	27.80
3	2	←	2	1		258936.171(010)	0.001	1.60E+00	20.00	2.56E+00	12.66
3	4	←	2	3		258936.171(010)	−0.015	3.43E+00	42.86	1.18E+01	58.18
3	2	←	2	2		258937.248(005)	−0.008	2.96E−01	3.70	8.78E−02	0.44
3		←	2		1^f	260224.8148(0008)					
3	3	←	2	3		260223.656(005)	0.008	2.96E−01	3.70	8.78E−02	0.44
3	3	←	2	2		260224.524(005)	0.012	2.37E+00	29.63	5.62E+00	27.80
3	2	←	2	1		260224.959(010)	0.046	1.60E+00	20.00	2.56E+00	12.66
3	4	←	2	3		260224.959(010)	0.006	3.43E+00	42.86	1.18E+01	58.18
3	2	←	2	2		260226.200(005)	0.007	2.96E−01	3.70	8.78E−02	0.44
4		←	3		1^e	345238.7124(0012)					
4	4	←	3	4		345237.419(005)	0.007	2.34E−01	2.08	5.49E−02	0.14
4	4	←	3	3		345238.583(005)	−0.006	3.52E+00	31.25	1.24E+01	30.34
4	3	←	3	2		345238.707(005)	−0.005	2.68E+00	23.81	7.17E+00	17.62
4	5	←	3	4		345238.790(005)	0.001	4.58E+00	40.74	2.10E+01	51.58
4	3	←	3	3		345240.214(005)	−0.006	2.34E−01	2.08	5.49E−02	0.14
4	4/5	←	3	4/4		345238.102(005)	0.002			7.23E−03	0.04
4	4/4	←	3	4/3		345238.008(005)	0.007			1.92E−02	0.10
4		←	3		1^f	346956.7907(0012)					
4	4	←	3	4		346955.364(005)	0.002	2.34E−01	2.08	5.49E−02	0.14
4	4	←	3	3		346956.661(005)	−0.006	3.52E+00	31.25	1.24E+01	30.34
4	3	←	3	2		346956.782(005)	0.000	2.68E+00	23.81	7.17E+00	17.62
4	5	←	3	4		346956.868(005)	−0.002	4.58E+00	40.74	2.10E+01	51.58
4	3	←	3	3		346958.463(005)	0.000	2.34E−01	2.08	5.49E−02	0.14
4	4/5	←	3	4/4		346956.110(005)	−0.006			2.02E−02	0.10
4	4/4	←	3	4/3		346956.015(005)	0.001			4.54E−02	0.22
5		←	4		1^e	431533.3534(0016)					
5	5	←	4	5		431531.923(005)	0.010	1.92E−01	1.33	3.69E−02	0.06
5	5	←	4	4		431533.320(010)	0.030	4.61E+00	32.00	2.12E+01	31.42
5	4	←	4	3		431533.320(010)	−0.014	3.73E+00	25.93	1.39E+01	20.62
5	6	←	4	5		431533.418(010)	0.015	5.67E+00	39.39	3.22E+01	47.62
5	4	←	4	4		431534.974(005)	0.010	1.92E−01	1.33	3.69E−02	0.06
5		←	4		1^f	433680.5135(0016)					
5	5	←	4	5		433678.940(005)	−0.002	1.92E−01	1.33	3.69E−02	0.06
5	5	←	4	4		433680.462(010)	0.012	4.61E+00	32.00	2.12E+01	31.42
5	4	←	4	3		433680.462(010)	−0.027	3.73E+00	25.93	1.39E+01	20.62
5	6	←	4	5		433680.570(010)	0.005	5.67E+00	39.39	3.22E+01	47.62
5	4	←	4	4		433682.282(005)	−0.003	1.92E−01	1.33	3.69E−02	0.06
5	4/5	←	4	4/4		433681.382(010)	0.015			2.06E−02	0.06
6		←	5		1^e	517817.9701(0022)					
6	6	←	5	5		517817.962(010)	0.030	5.67E+00	32.41	3.22E+01	31.98
6	5	←	5	4		517817.962(010)	0.015	4.77E+00	27.27	2.28E+01	22.64
6	7	←	5	6		517817.962(010)	−0.043	6.73E+00	38.46	4.53E+01	45.04
6	6/7	←	5	6/6		517817.200(010)	−0.024			6.52E−02	0.12
6	5/6	←	5	5/5		517818.784(005)	0.008			3.28E−02	0.06
6		←	5		1^f	520393.9207(0022)					
6	6	←	5	6		520392.254(005)	−0.005	1.62E−01	0.93	2.63E−02	0.02
6	6	←	5	5		520393.899(010)	0.017	5.67E+00	32.41	3.22E+01	31.98
6	5	←	5	4		520393.899(010)	0.005	4.77E+00	27.27	2.28E+01	22.64
6	7	←	5	6		520393.965(010)	0.008	6.73E+00	38.46	4.53E+01	45.04
6	5	←	5	5		520395.724(005)	−0.006	1.62E−01	0.93	2.63E−02	0.02
6	6/7	←	5	6/6		520393.073(010)	−0.035			1.11E−01	0.22
6	6/5	←	5	5/5		520394.820(010)	0.014			6.42E−02	0.12
7		←	6		1^e	604090.5584(0028)					
7	7	←	6	7		604088.974(005)	0.005	1.40E−01	0.68	1.96E−02	0.02
7	7	←	6	6		604090.544(010)	0.011	6.72E+00	32.65	4.51E+01	32.30
7	6	←	6	5		604090.544(010)	0.009	5.80E+00	28.21	3.37E+01	24.10
7	8	←	6	7		604090.544(010)	−0.041	7.77E+00	37.78	6.04E+01	43.22
7	6	←	6	6		604092.220(005)	−0.005	1.40E−01	0.68	1.96E−02	0.02
7	7/8	←	6	7/7		604089.767(005)	−0.010			1.20E−01	0.18
7	7/6	←	6	6/6		604091.379(005)	0.000			8.11E−02	0.12
7		←	6		1^f	607094.9499(0028)					
7	7	←	6	7		607093.232(005)	0.007	1.40E−01	0.68	1.96E−02	0.02
7	7	←	6	6		607094.951(010)	0.027	6.72E+00	32.65	4.51E+01	32.30
7	6	←	6	5		607094.951(010)	0.026	5.80E+00	28.21	3.37E+01	24.10
7	8	←	6	7		607094.951(010)	−0.027	7.77E+00	37.78	6.04E+01	43.22
7	6	←	6	6		607096.770(005)	−0.002	1.40E−01	0.68	1.96E−02	0.02
7	7/8	←	6	7/7		607094.093(005)	−0.008			1.81E−01	0.26
7	6/7	←	6	6/6		607095.852(005)	0.004			1.32E−01	0.18
8		←	7		1^e	690349.1143(0037)					
8	7	←	7	6		690349.108(010)	0.016	6.82E+00	28.89	4.66E+01	25.18
8	8	←	7	7		690349.108(010)	0.012	7.75E+00	32.81	6.01E+01	32.50

Table 2. (continued).

J'	F'	←	J''	F''	υ_2	ν (σ) / MHz	Diff. / MHz	${}^{A}I_{\rm lin}$	${}^{R}I_{\rm lin}$	${}^{A}I_{\rm sat}$	${}^{R}I_{\rm sat}$
8	9	←	7	8		690349.108(010)	−0.028	8.80E+00	37.25	7.75E+01	41.88
8	8/9	←	7	8/8		690348.299(005)	−0.009			1.85E−01	0.20
8	7/8	←	7	7/7		690349.943(005)	0.003			1.48E−01	0.16
8		←	7		1^f	693781.5395(0037)					
8	7	←	7	6		693781.535(010)	0.019	6.82E+00	28.89	4.66E+01	25.18
8	8	←	7	7		693781.535(010)	0.014	7.75E+00	32.81	6.01E+01	32.50
8	9	←	7	8		693781.535(010)	−0.027	8.80E+00	37.25	7.75E+01	41.88
8	8/9	←	7	8/8		693780.654(005)	−0.011			2.56E−01	0.28
8	7/8	←	7	7/7		693782.451(005)	0.011			1.87E−01	0.20
9		←	8		1^e	776591.6344(0048)					
9	8	←	8	7		776591.632(010)	0.019	7.84E+00	29.41	6.15E+01	26.04
9	9	←	8	8		776591.632(010)	0.012	8.78E+00	32.92	7.71E+01	32.64
9	10	←	8	9		776591.632(010)	−0.020	9.82E+00	36.84	9.65E+01	40.86
9	9/10	←	8	9/9		776590.796(005)	−0.012			2.54E−01	0.22
9	8/9	←	8	8/8		776592.466(005)	0.005			2.23E−01	0.18
9		←	8		1^f	780451.6283(0048)					
9	8	←	8	7		780451.625(010)	0.019	7.84E+00	29.41	6.15E+01	26.04
9	9	←	8	8		780451.625(010)	0.011	8.78E+00	32.92	7.71E+01	32.64
9	10	←	8	9		780451.625(010)	−0.022	9.82E+00	36.84	9.65E+01	40.86
9	9/10	←	8	9/9		780450.726(005)	−0.007			3.29E−01	0.28
9	8/9	←	8	8/8		780452.533(005)	0.002			2.98E−01	0.26
10		←	9		1^e	862816.1156(0061)					
10	9	←	9	8		862816.117(010)	0.022	8.86E+00	29.82	7.85E+01	26.74
10	10	←	9	9		862816.117(010)	0.013	9.80E+00	33.00	9.61E+01	32.74
10	11	←	9	10		862816.117(010)	−0.014	1.08E+01	36.51	1.18E+02	40.06
10		←	9		1^f	867103.1558(0061)					
10	9	←	9	8		867103.154(010)	0.019	8.86E+00	29.82	7.85E+01	26.74
10	10	←	9	9		867103.154(010)	0.010	9.80E+00	33.00	9.61E+01	32.74
10	11	←	9	10		867103.154(010)	−0.018	1.08E+01	36.51	1.18E+02	40.06
11		←	10		1^e	949020.5552(0078)					
11	10	←	10	9		949020.557(010)	0.021	9.87E+00	30.16	9.74E+01	27.32
11	11	←	10	10		949020.557(010)	0.011	1.08E+01	33.06	1.17E+02	32.82
11	12	←	10	11		949020.557(010)	−0.012	1.19E+01	36.23	1.41E+02	39.42
11		←	10		1^f	953734.0621(0078)					
11	10	←	10	9		953734.063(010)	0.021	9.87E+00	30.16	9.74E+01	27.32
11	11	←	10	10		953734.063(010)	0.011	1.08E+01	33.06	1.17E+02	32.82
11	12	←	10	11		953734.063(010)	−0.013	1.19E+01	36.23	1.41E+02	39.42
21		←	20		1^e	1809522.5616(0599)					
21	20	←	20	19		1809522.600(050)	0.070	1.99E+01	31.71	3.97E+02	30.14
21	21	←	20	20		1809522.600(050)	0.059	2.09E+01	33.26	4.37E+02	33.16
21	22	←	20	21		1809522.600(050)	0.047	2.19E+01	34.88	4.81E+02	36.48
21		←	20		1^f	1818456.4978(0599)					
21	20	←	20	19		1818456.454(050)	−0.011	1.99E+01	31.71	3.97E+02	30.14
21	21	←	20	20		1818456.454(050)	−0.022	2.09E+01	33.26	4.37E+02	33.16
21	22	←	20	21		1818456.454(050)	−0.035	2.19E+01	34.88	4.81E+02	36.48
22		←	21		1^e	1895374.5705(0714)					
22	21	←	21	20		1895374.516(050)	−0.015	2.09E+01	31.78	4.38E+02	30.28
22	22	←	21	21		1895374.516(050)	−0.026	2.19E+01	33.26	4.80E+02	33.16
22	23	←	21	22		1895374.516(050)	−0.038	2.29E+01	34.81	5.26E+02	36.34
23		←	22		1^e	1981182.5655(0847)					
23	22	←	22	21		1981182.553(050)	0.036	2.19E+01	31.85	4.81E+02	30.42
23	23	←	22	22		1981182.553(050)	0.025	2.29E+01	33.27	5.25E+02	33.18
23	24	←	22	23		1981182.553(050)	0.013	2.39E+01	34.75	5.73E+02	36.20
23		←	22		1^f	1990948.0839(0847)					
23	22	←	22	21		1990948.036(050)	0.001	2.19E+01	31.85	4.81E+02	30.42
23	23	←	22	22		1990948.036(050)	−0.010	2.29E+01	33.27	5.25E+02	33.18
23	24	←	22	23		1990948.036(050)	−0.022	2.39E+01	34.75	5.73E+02	36.20

Table 3. Newly measured high J direct l-type transitions of $H^{13}CN$ in the first excited bending state. Experimental uncertainties (one standard deviation) and the differences between observed and calculated transition frequencies are given in MHz.

J'	l'	J''	l''	$\nu_{\rm exp}$ /MHz	σ / MHz	o-c / MHz
19	f	19	e	81288.914	0.020	0.005
20	f	20	e	89805.251	0.020	0.002
28	f	28	e	172863.280	0.010	−0.008
29	f	29	e	185090.975	0.010	0.000
30	f	30	e	197723.753	0.010	0.005
31	f	31	e	210759.976	0.020	−0.005
32	f	32	e	224197.976	0.025	0.015
33	f	33	e	238036.001	0.020	0.012
34	f	34	e	252272.301	0.020	0.021
35	f	35	e	266904.987	0.020	−0.027

niques, yielding most accurate information about the hyperfine structure with sub-Doppler precision. The ground vibrational state $H^{13}CN$ data are given in Table 1, and the first excited state in Table 2. Direct l-type transitions of $H^{13}CN$ were measured for the first time between 81 and 267 GHz (up to $J = 35$), and are listed in Table 3. In the first paper of this HCN series [2] we discussed the main features of the rotational spectrum of $H^{12}CN$, including the effects of hyperfine, (eqQ), spin-rotation, ($C_I(^{14}N)$), and possibly spin-spin interaction. We follow this approach for the new data set of the ^{13}C isotopomer and, analogously to the display of the $H^{12}CN$ data in Fig. 2 of [2], we present here some of the rotational transition profiles of $H^{13}CN$ (see Figs. 1.1 – 1.3). Since the various interaction parameters of $H^{12}CN$ are nearly identical to those of $H^{13}CN$, their rotational spectra are nearly identical, if one considers the frequency shift due to the different isotopic substitution appropriately.

We have extended our studies to the ^{15}N isotopomers $H^{12}C^{15}N$ and $H^{13}C^{15}N$. All measured transitions for the ground and first vibrational excited state of $H^{12}C^{15}N$ are presented in Table 4, whereas Table 5 contains data of the $H^{13}C^{15}N$ isotopomer.

3.1. The $H^{13}CN$ Isotopomer

Sub-Doppler Measurements: Lamb Dips and Crossover Dips

It is well known that the power saturation of the purely Doppler broadened line profile produces a fairly narrow (about 40 kHz) dip at the center of the transition. In addition to the Lamb dips, which are always present, crossover-dips can occur only if two conditions are met simultaneously: *(i)* the participating transitions have to share an energy level, and *(ii)* the level separation has to be within the Doppler width. This latter condition is fulfilled for most R-branch transitions which are presented here (see Fig. 1.3). The theory of Lamb dips and crossover dips has been worked out by Oka and collaborators [15, 16], and has been applied to the discussion of numerous spectra, particularly also to the $H^{12}CN$ data [2].

Table 4. Sub-Doppler rotational transitions of $H^{12}C^{15}N$ in the ground and first excited bending vibrational state. The estimated error for transitions up to $J = 10$ is below 10 kHz. Transitions above 1 THz have been measured in Doppler limited resolution with 1 σ errors of 50 kHz. For each transition the difference between observed and calculated frequency is given.

J'	←	J''	υ_2	ν / MHz	o-c./ MHz
1	←	0	0	86054.967	0.0003
2	←	1	0	172107.956	−0.0017
3	←	2	0	258157.009	0.0116
4	←	3	0	344200.093	−0.0174
5	←	4	0	430235.310	−0.0114
6	←	5	0	516260.657	0.0018
7	←	6	0	602274.137	0.0010
8	←	7	0	688273.793	0.0018
9	←	8	0	774257.651	0.0058
10	←	9	0	860223.721	−0.0040
11	←	10	0	946170.057	−0.0008
21	←	20	0	1804113.688	0.0536
22	←	21	0	1889712.655	−0.0571
23	←	22	0	1975268.438	0.0147
2	←	1	1e	172093.067	0.0099
2	←	1	1f	172940.761	0.0066
3	←	2	1e	258134.608	0.0006
3	←	2	1f	259406.006	−0.0018
4	←	3	1e	344170.176	−0.0080
4	←	3	1f	345865.101	−0.0119
5	←	4	1e	430197.801	0.0051
5	←	4	1f	432316.022	0.0015
6	←	5	1e	516215.453	0.0007
6	←	5	1f	518756.686	0.0041
7	←	6	1e	602221.163	0.0004
7	←	6	1f	605185.050	0.0011
8	←	7	1e	688212.938	0.0012
8	←	7	1f	691599.077	0.0036
9	←	8	1e	774188.786	0.0011
9	←	8	1f	777996.706	−0.0023
10	←	9	1e	860146.710	−0.0076
10	←	9	1f	864375.906	−0.0009
11	←	10	1e	946084.751	0.0050
11	←	10	1f	950734.624	0.0008
21	←	20	1e	1803933.219	0.0311
21	←	20	1f	1812745.805	−0.0412
22	←	21	1e	1889521.171	−0.0228
22	←	21	1f	1898744.560	0.0432
23	←	22	1e	1975065.498	0.0121
23	←	22	1f	1984698.208	−0.0323

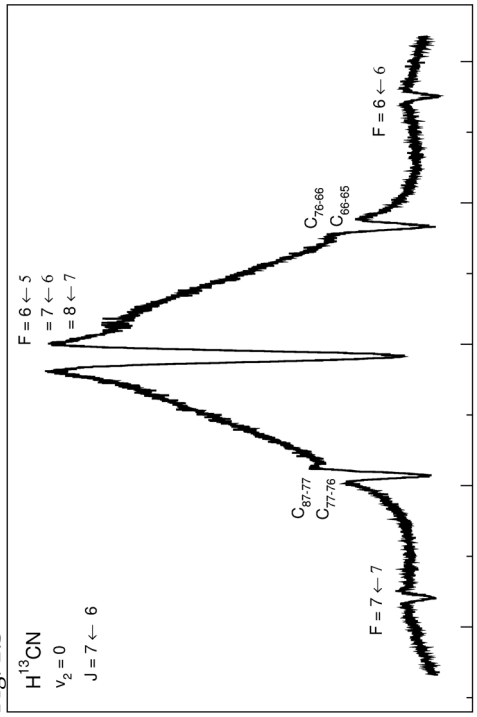

Fig. 1.3

Fig. 1.1. The vibrational ground state $J = 2 \leftarrow 1$ transition of $H^{13}CN$ in Doppler (upper trace) and sub Doppler resolution (lower trace). The 6 hyperfine components are clearly resolved, although $\Delta F = -1$ transitions are weak and thus the $F = 1 \leftarrow 2$ Lamb dip is just on the limit of detection.

Fig. 1.2. Spectrum of the vibrational ground state $J = 3 \leftarrow 2$ transition of $H^{13}CN$. For large modulation amplitudes the $F = 3 \leftarrow 2$ and the $F = 4 \leftarrow 3$ Lamb dip transitions are not resolved. The effect of modudaltion broadening is partly lifted at moderate amplitudes (see magnification).

Fig. 1.3. The $J = 7 \leftarrow 6$ ground state rotational transition of $H^{13}CN$. The $\Delta F = +1$ components line up to one strong single transition. Beside weaker $\Delta F = 0$ components, strong cross over dips, $C_{FbFb''-Fa'Fa''}$, are centered between corresponding $\Delta F = +1$ and $\Delta F = 0$ components.

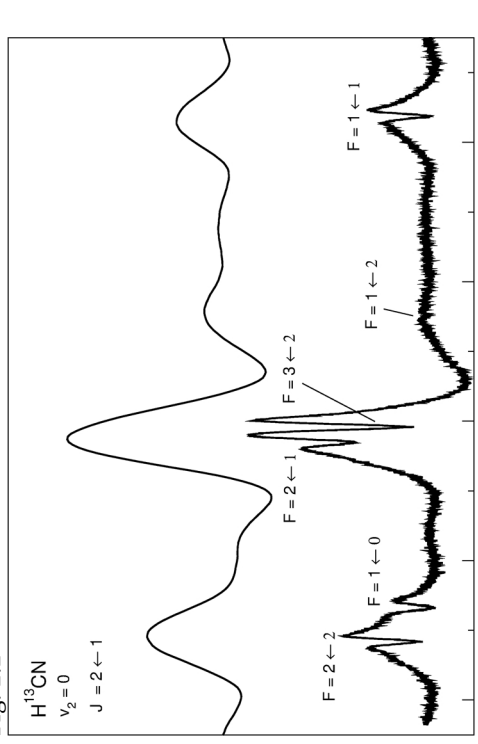

Fig. 1.1

Fig. 1.2

Table 5. Sub-Doppler rotational transitions of $H^{13}C^{15}N$ in the ground and first excited bending vibrational state. The estimated error for transitions up to $J = 10$ is below 10 kHz. Transitions above 1 THz have been measured in Doppler limited resolution with 1 σ errors of 50 kHz. For each transition the difference between observed and calculated frequency is given.

J'	$\leftarrow$	J''	υ_2	ν / MHz	o-c. / MHz
1	$\leftarrow$	0	0	83727.577	−0.0008
2	$\leftarrow$	1	0	167453.279	−0.0008
3	$\leftarrow$	2	0	251175.242	0.0116
4	$\leftarrow$	3	0	334891.540	−0.0140
5	$\leftarrow$	4	0	418600.372	−0.0033
6	$\leftarrow$	5	0	502299.823	0.0041
7	$\leftarrow$	6	0	585988.016	0.0059
8	$\leftarrow$	7	0	669663.068	−0.0061
9	$\leftarrow$	8	0	753323.142	0.0052
10	$\leftarrow$	9	0	836966.329	0.0047
11	$\leftarrow$	10	0	920590.758	−0.0053
21	$\leftarrow$	20	0	1755392.359	0.0514
22	$\leftarrow$	21	0	1838687.111	0.0457
23	$\leftarrow$	22	0	1921940.618	−0.0338
24	$\leftarrow$	23	0	2005151.181	−0.0237
2	$\leftarrow$	1	1e	167411.171	0.0075
2	$\leftarrow$	1	1f	168220.495	−0.0172
3	$\leftarrow$	2	1e	251112.025	0.0008
3	$\leftarrow$	2	1f	252325.913	−0.0018
4	$\leftarrow$	3	1e	334807.209	−0.0109
4	$\leftarrow$	3	1f	336425.490	−0.0034
5	$\leftarrow$	4	1e	418494.863	0.0008
5	$\leftarrow$	4	1f	420517.311	0.0040
6	$\leftarrow$	5	1e	502173.065	0.0017
6	$\leftarrow$	5	1f	504599.416	0.0011
7	$\leftarrow$	6	1e	585839.943	0.0074
7	$\leftarrow$	6	1f	588669.866	−0.0107
8	$\leftarrow$	7	1e	669493.586	−0.0055
8	$\leftarrow$	7	1f	672726.760	0.0076
9	$\leftarrow$	8	1e	753132.146	0.0020
9	$\leftarrow$	8	1f	756768.105	0.0023
10	$\leftarrow$	9	1e	836753.710	0.0035
10	$\leftarrow$	9	1f	840791.988	−0.0005
11	$\leftarrow$	10	1e	920356.389	−0.0038
11	$\leftarrow$	10	1f	924796.471	−0.0005
21	$\leftarrow$	20	1f	1763348.311	−0.0069
22	$\leftarrow$	21	1e	1838201.221	−0.0156
22	$\leftarrow$	21	1f	1847011.707	0.0137
23	$\leftarrow$	22	1e	1921430.520	0.0101
23	$\leftarrow$	22	1f	1930632.475	−0.0059
24	$\leftarrow$	23	1e	2004616.450	0.0015

As an example for the occurrence of saturation dips we compare the traces of several line profiles of $H^{12}CN$ (see Fig. 2 of [2]) and $H^{13}CN$ (see Fig. 1) for different rotational transitions: $J = 2 \leftarrow 1$, $J = 3 \leftarrow 2$, and $J = 7 \leftarrow 6$ in the vibrational ground state.

The trace of the $J = 2 \leftarrow 1$ transition in Fig. 1.1 represents the absorption profile with the Lamb dips at 172 678 MHz center frequency. A total of 6 hyperfine components is expected, but usually only 5 are clearly identified. The 6$^{\text{th}}$ hyperfine component $F = 1 \leftarrow 2$ is the weakest and carries only about 0.6% of the transition's total intensity. However, we have tentatively marked the frequency position of the $F = 1 \leftarrow 2$ line. It is just on the limit of detection. It may be noticed that the $J = 2 \leftarrow 1$ absorption profile consists only of saturation dips, but no crossover dips. Similarly, the $J = 3 \leftarrow 2$ transition in Fig. 1.2. also shows only saturation dips, and no crossover dips, a fact that finds its explanation in a frequency separation larger than the Doppler width of the individual F components. The recorded Doppler profiles for the transitions $J = 2 \leftarrow 1$ and $3 \leftarrow 2$ are printed above the saturation absorption trace. In our $H^{12}CN$ paper [2] we have given as an example the energy level scheme of the $J = 7 \leftarrow 6$ transition (see Fig. 2.5 of [2]). Accordingly we show in Fig. 1.3 the $7 \leftarrow 6$ transition of $H^{13}CN$ in sub-Doppler resolution. We want to pick out this transition once more to discuss the sub-Doppler spectrum in detail. Each rotational level, i. e. $J = 6$ and $J = 7$, is split by the hyperfine interaction into three hyperfine levels. Together with the hyperfine selection rules ($\Delta F = 0, \pm 1$), one expects for each rotational transition a splitting into 6 hyperfine components. As aforementioned, the $\Delta F = -1$ component is usually too weak to be observed. Therefore, $J = 7 \leftarrow 6$ splits into 5 components, where the stronger ones follow $\Delta F = +1$ with $F = 8 \leftarrow 7$, $7 \leftarrow 6$, $6 \leftarrow 5$, and the two weaker components $\Delta F = 0$ with the two components $F = 7 \leftarrow 7$, $6 \leftarrow 6$. In addition, crossover-dips show up clearly, occuring as two paired, overlapping transitions, C_{87-77} / C_{77-76} and C_{76-66} / C_{66-65} (see [2] for details on the notation).

First vibrational excited state

Like most linear polyatomic molecules with a closed electronic shell, HCN exhibits an $^1\Sigma$ electronic ground state. The bending vibration υ_2 displays two degenerated first excited states, $\upsilon_2 = 1^e$ and $\upsilon_2 = 1^f$, which have a vibrational angular momentum $|l| = 1$ along the molecular axis. The l-type degeneracy is lifted by Coriolis interaction of the vibrational and the rotational angular momentum. Figures 2.1 and 2.2 show the $J = 3 \leftarrow 2$ transition in the $\upsilon_2 = 1^e$ and $\upsilon_2 = 1^f$ state. The pattern of hyperfine transitions looks almost the same for the ground (see Fig. 1.2) and the two excited bending states, although the relative positions of the $F = 2 \leftarrow 1$ and the $F = 3 \leftarrow 2$ transition are exchanged.

Fig. 2.1

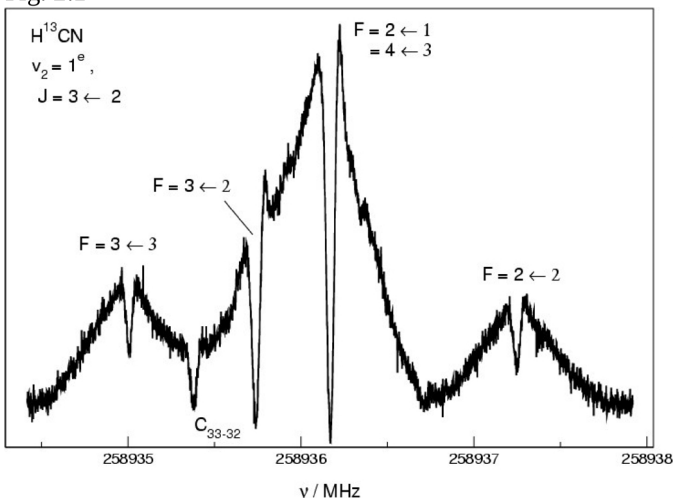

Fig. 2.1. $H^{13}CN$ first excited state ($\upsilon_2 = 1^f$): Lamb dip spectrum of the $J = 3 \leftarrow 2$ rotational transition.

Fig. 2.2

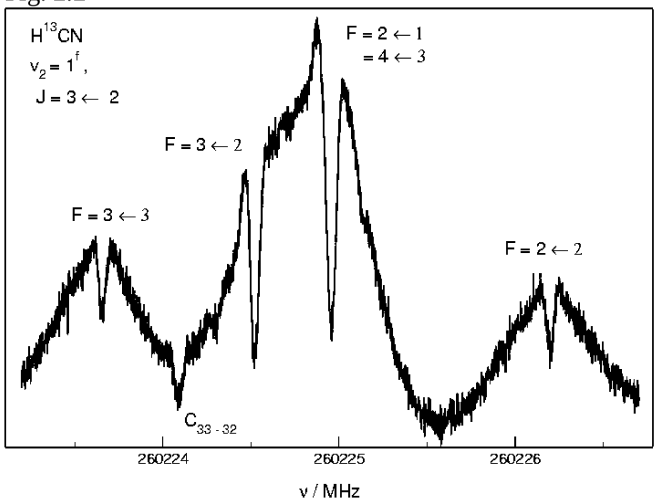

Fig. 2.2. $H^{13}CN$ first excited state ($\upsilon_2 = 1^e$): Lamb dip spectrum of the $J = 3 \leftarrow 2$ rotational transition.

Fig. 3

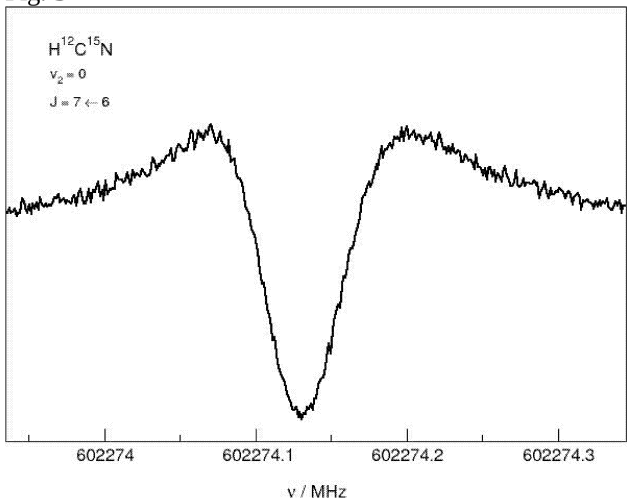

Fig. 3. Ground state $J = 7 \leftarrow 6$ rotational transition of $H^{12}C^{15}N$ in sub-Doppler resolution. The hyperfine splitting is too small to be resolved.

Fig. 4

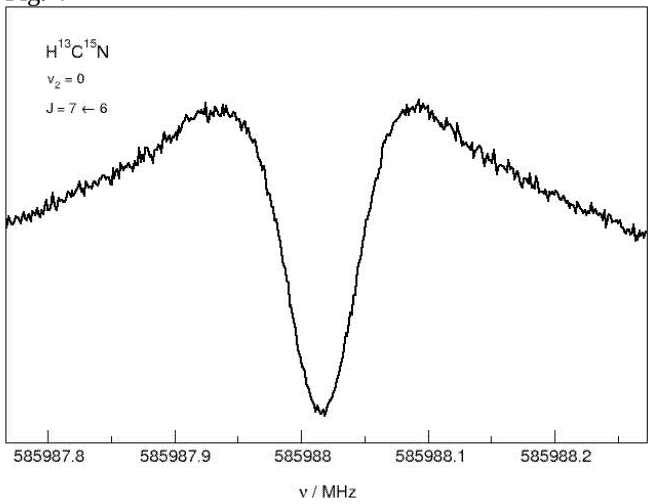

Fig. 4. Ground state $J = 7 \leftarrow 6$ rotational transition of $H^{13}C^{15}N$ in sub-Doppler resolution. The hyperfine splitting is too small to be resolved.

Direct l-type transitions in the excited bending vibrational mode are Q-branch transitions which obey the selection rule $J, f \leftarrow J, e$. We have measured 10 new lines with quantum numbers $J = 19, 20, 28, \ldots, 35$ (see Table 3). These transitions do not contain any information on the rotational constant B, but allow the evaluation of the l-type doubling constant q and its centrifugal distortion corrections with high accuracy.

3.2. The $H^{12}C^{15}N$ and $H^{13}C^{15}N$ Isotopomers

Because of the zero electric nuclear quadrupole moment of ^{15}N, the two isotopic species $H^{12}C^{15}N$ and $H^{13}C^{15}N$ do not exhibit a measurable hyperfine structure. The spectra up to 900 GHz were nevertheless recorded in sub-Doppler resolution, with the objective of improved frequency accuracy (a factor of 5–10 for most lines). As examples we show in Figs. 3 and 4 spectra of the $H^{12}C^{15}N$ and $H^{13}C^{15}N$ $J = 7 \leftarrow 6$ transitions in sub-Doppler resolution. Above 1 THz all the lines were measured in Doppler-limited resolution with estimated errors of about 50 kHz. Possible nuclear spin-rotation, and spin-spin interaction splittings due to the magnetic moments of H, ^{13}C and ^{15}N were not resolved in our experiments. We performed, however, calculations including the interaction of all participating nuclei. The corresponding constants have been calculated from the nuclear spin-rotation constants of hydrogen-cyanide published by Garvey and De Lucia [17]. The found splitting of the strong hyperfine components lies with a few kHz well below the achieved sub-Doppler resolution. Although this splitting is not resolved, it might cause a substantial broadening of the lines.

4. Analysis

The energy expression of a linear molecule with a degenerated bending mode including hyperfine interaction can be written as [18]:

$$\begin{aligned}\frac{E^{\pm}}{h} &= \frac{E_{\upsilon,\mathrm{vib}}}{h} + \frac{E_{\upsilon,\mathrm{rot}}}{h} + \frac{E_{\upsilon,\mathrm{HFS}}}{h} \\ &= G_\upsilon + B_\upsilon[J(J+1) - l^2] - D_\upsilon[J(J+1) - l^2]^2 \\ &\quad + H_\upsilon[J(J+1) - l^2]^3 \pm \frac{q}{2}J(J+1) \mp \frac{q_J}{2}J^2(J+1)^2 \\ &\quad \pm \frac{q_{JJ}}{2}J^3(J+1)^3 \pm \frac{q_{JJJ}}{2}J^4(J+1)^4 \\ &\quad + eQq_\upsilon Y(J,I,F)\Big[\frac{3l^2}{J(J+1)} - 1 \pm \frac{\eta}{2}\Big] + \frac{C_{I,\upsilon}}{2}C.\end{aligned}$$

Here B, D, H denote the rotational spectroscopic constants, eQq is the nuclear electric quadrupole coupling constant, C_I the magnetic spin-rotation coupling constant, $\boldsymbol{F} = \boldsymbol{J} + \boldsymbol{I}$ the total angular momentum,

$$Y(J,I,F) = \frac{\frac{3}{4}C(C+1) - I(I+1)J(J+1)}{2(2J-1)(2J+3)I(2I-1)}$$

and $C = F(F+1) - J(J+1) - I(I+1)$ Casimir's function. Furthermore, for vibrational excited states the l-type doubling constant q, its centrifugal distortion corrections q_J, q_{JJ} and q_{JJJ} and the asymmetry parameter η have to be considered. The value of the last parameter can be deduced from the parameter $eQq\eta = eQq_1 \times \eta$, which is given in Table 6. The subscript v denotes the vibrational quantum number. According to the scheme proposed by Brown et al. [19] the rotational sub-levels of the first excited bending mode are labeled as e and f, where the e levels are energetically lower than the corresponding f levels. The rotational energy levels in the (01^e0) state are designated E^-, those in the (01^f0) state E^+.

For $H^{13}CN$ and $H^{15}CN$, data of the $v = 0$ ground state and $v = 1$ first excited bending states have been included in a simultaneous fit together with infrared data of the bending fundamental published by Maki et al. (2000) [20]. For these two isotopomers, the band center frequency of the lowest bending mode, $\Delta E = G_1 - G_0$, could be derived. To our knowledge there exist no ro-vibrational data on the lowest bending mode of $H^{13}C^{15}N$. Therefore we performed a separate fit of the ground and first excited bending state in this case. For all three isotopomers, also data on direct l-type transitions between 8 and 52 GHz have been included in the fit [9].

The derived, highly precise spectroscopic constants of all isotopomers can be found in Tables 6–8.

Because of the large ^{14}N electric quadrupole moment, the hyperfine splitting of $H^{13}C^{14}N$ is clearly resolved, and the magnetic spin rotational constant $C_I(^{14}\mathrm{N})$ could be determined for the first time. The splitting of energy levels induced by any other coupling constants could not be resolved, and the corresponding interactions where thus neglected in the analysis.

5. Results and Conclusions

The most reliable set of molecular and hyperfine constants so far for $H^{13}CN$ and the ^{15}N-isotopomers $H^{12}C^{15}N$ and $H^{13}C^{15}N$ have been derived in this work.

Table 6. Molecular constants of $H^{13}CN$ received from a simultaneous fit of the ground and first excited vibrational state. The reference value of *eQq* for the first excited state from Preusser and Maki is the mean value of their quoted constant *eQq* for the *e* and *f* state.

$H^{13}CN$ ($v_2 = 0,1$)				
Parameter		This work	— Previous work —	
Ground vibrational state:				
B_0	/MHz	43170.12635(17)	43170.1281(21)	Maki et al. [20]
D_0	/kHz	82.98716(81)	82.9987(53)	Maki et al. [20]
H_0	/Hz	0.07922(67)	0.0810(17)	Maki et al. [20]
eQq_0	/MHz	−4.7070(32)	−4.737(28)	Preusser et al. [7]
$C_{I,0}(^{14}N)$	/kHz	9.62(38)	–	
First excited vibrational state:				
B_1	/MHz	43264.761416(150)	43264.7639(17)	Maki et al. [20]
D_1	/kHz	84.76127(81)	84.7735(57)	Maki et al. [20]
H_1	/Hz	0.09479(78)	0.0963(19)	Maki et al. [20]
q	/MHz	214.837624(51)	214.83712(39)	Maki et al. [20]
q_J	/kHz	2.43375(30)	2.4305(17)	Maki et al. [20]
q_{JJ}	/Hz	0.03757(45)	0.03402(54)	Maki et al. [20]
$q_{JJJ} \cdot 10^6$	/Hz	0.684(20)	–	–
eQq_1	/MHz	−4.8097(31)	−4.833(45)	Maki et al. [20]
eQq_η	/MHz	0.0966(13)	–	–
$C_{I,1}(^{14}N)$	/kHz	9.78(34)	–	–
ΔE	/cm^{-1}	707.408878(11)	707.408891(21)	Maki et al. [20]
weighted rms		0.92		

Table 7. Molecular constants of $HC^{15}N$ obtained by a simultaneous fit of the ground and first excited vibrational state.

$H^{12}C^{15}N$ ($v_2 = 0,1$)			
Parameter		This work	Previous work (Maki et al. [20])
Ground vibrational state:			
B_0	/MHz	43027.64798(21)	43027.6516(22)
D_0	/kHz	82.3202(12)	82.3404(60)
H_0	/Hz	0.0770(13)	0.0859(19)
First excited vibrational state:			
B_1	/MHz	43129.73155(18)	43129.7334(13)
D_1	/kHz	84.1854(12)	84.204(57)
H_1	/Hz	0.0935(14)	0.1021(19)
q	/MHz	211.94375(25)	211.943645(87)
q_J	/kHz	2.4272(15)	2.4258(11)
q_{JJ}	/Hz	0.0385(15)	0.03568(42)
$q_{JJJ} \cdot 10^6$	/Hz	0.69(34)	–
ΔE	/cm^{-1}	712.465156(12)	712.465207(23)
weighted rms		0.76	

A simultaneous fit to a selected set of high precision measurements to the energy expression of a linear molecule has been performed. In addition to *B*, *D*, and *H* we determined for the $H^{13}CN$ isotopomer the electric quadrupole coupling constant (*eQq*), the asymmetry parameter η, and the magnetic spin rotation constant C_I (^{14}N). For the other examined species, the hyperfine structure due to the H, ^{13}C, and ^{15}N nuclear spin could not be resolved. However, the newly received data set includes rotational transitions of three HCN isotopomers up to $J = 24 \leftarrow 23$ (at around 2 THz) in the ground and first excited vibrational bending state with high frequency accuracy. Furthermore, the combination of existing data and the newly measured transitions represents the most comprehensive data set to date, with yet unprecedented high accuracy at high frequencies.

This is of importance for astrophysical observations, since with the future satellite mission Herschel and the Stratospheric Observatorium for Infrared Astronomy (SOFIA) high resolution observations up to 2 THz will be possible. With this new data set it is now possible to predict transition frequencies of the $H^{13}CN$, $HC^{15}N$ and $H^{13}C^{15}N$ isotopomers up to 2.5 THz with frequency uncertainty of less than 100 kHz. The newly calculated line predictions will be implemented in the Cologne Database for Molecular Spectroscopy (CDMS) at *www.cdms.de* [10] and thus be freely available for the spectroscopical and astronomical community.

Table 8. Molecular constants of $H^{13}C^{15}N$ obtained by separate fits of the ground and first excited vibrational state.

Parameter		$H^{13}C^{15}N$ ($v_2 = 0,1$) This work	— Previous work —	
Ground vibrational state:				
B_0	/MHz	41863.94519(33)	41863.9461(83)	Pearson et al. [8]
D_0	/kHz	78.15607(224)	78.15(21)	Pearson et al. [8]
H_0	/Hz	0.07434(262)	–	–
First excited vibrational state:				
B_1	/MHz	41954.4021(20)	41954.4418(57)	Preusser et al. [7]
D_1	/kHz	79.7892(14)	79.829(147)	Preusser et al. [7]
H_1	/Hz	0.0825(16)	–	–
q	/MHz	202.35482(32)	202.35443(79)	Preusser et al. [7]
q_J	/kHz	2.208(22)	2.2001(42)	Preusser et al. [7]
q_{JJ}	/Hz	0.0286(25)	–	–
	weighted rms $v_2 = 0$	0.90		
	weighted rms $v_2 = 1$	0.86		

Acknowledgements

The Cologne group has been supported by the Deutsche Forschungsgemeinschaft via research grant SFB-494. We much acknowledge the Ministry of Science of the Land Nordrhein-Westfalen, Germany, for financial support. Štepan Urban acknowledges support through the Grant Agency of the Czech Republic (#203/01/1274). The collaborative work between the groups of Štepan Urban, Prague, and the spectroscopy group in Cologne has been additionally supported by the International Office of the Federal Ministry of Education and Science at the DLR via grant CZE 00/030. The work carried out on the high power BWOs by ISTOK in collaboration with the Cologne group has been supported by the Deutsche Forschungsgemeinschaft through a grant aimed to support Eastern and Central European Countries and Republics of the Former SU. All support is greatly appreciated.

[1] S. Thorwirth, F. Wyrowski, P. Schilke, K. M. Menten, S. Brünken, H. S. P. Müller, and G. Winnewisser, Astrophys. J. **586**, 338 (2003).
[2] V. Ahrens, F. Lewen, S. Takano, G. Winnewisser, S. Urban, A. A. Negirev, and A. N. Koroliev, Z. Naturforsch. **57a**, 669 (2002).
[3] S. Thorwirth, H. S. P. Müller, F. Lewen, S. Brünken, V. Ahrens, and G. Winnewisser, Astrophys. J. **585**, L163 (2003).
[4] F. Maiwald, F. Lewen, V. Ahrens, M. Beaky, R. Gendriesch, A. N. Koroliev, A. A. Negirev, D. G. Paveljev, B. Vowinkel, and G. Winnewisser, J. Mol. Spectrosc. **202**, 166 (2000).
[5] Z. Zelinger, T. Amano, V. Ahrens, S. Brünken, F. Lewen, H. S. P. Müller, and G. Winnewisser, J. Mol. Spectrosc. **220**, 223 (2003).
[6] S. Brünken, U. Fuchs, F. Lewen, S. Urban, T. Giesen, and G. Winnewisser, J. Mol. Spectrosc. **225**, 152 (2004).
[7] J. Preusser and A. G. Maki, J. Mol. Spectrosc. **162**, 484 (1993).
[8] E. F. Pearson, R. A. Creswell, M. Winnewisser, and G. Winnewisser, Z. Naturforsch. **31a**, 1394 (1976).
[9] M. Winnewisser and J. Vogt, Z. Naturforsch. **33a**, 1323 (1978).
[10] H. S. P. Müller, S. Thorwirth, D. A. Roth, and G. Winnewisser, Astronomy and Astrophysics **370**, L49 (2001).
[11] M. Winnewisser, H. Lichau, and F. Wolf, J. Mol. Spectrosc. **202**, 155 (2000).
[12] G. Winnewisser, Vib. Spectrosc. **8**, 241 (1995).
[13] F. Lewen, E. Michael, R. Gendriesch, J. Stutzki, and G. Winnewisser, J. Mol. Spectrosc. **183**, 207 (1997).
[14] R. Gendriesch, F. Lewen, G. Winnewisser, and J. Hahn, J. Mol. Spectrosc. **203**, 205 (2000).
[15] T. Oka, Frontiers in Laser Spectroscopy, in R. Balian, S. Haroche, and S. Lieberman, (eds.), 531, North Holland, Amsterdam 1977.
[16] G. Magerl, W. Schupita, J. M. Frye, W. A. Kreiner, and T. Oka, J. Mol. Spectrosc. **107**, 72 (1984).
[17] R. M. Garvey, F. C. DeLucia, J. Mol. Spectrosc **50**, 38 (1974).
[18] N. van-Thanh and I. Rossi, J. Mol. Spectrosc. **157**, 68 (1993) .
[19] J. M. Brown, J. T. Hougen, K. P. Huber, J. W. C. Johns, I. Kopp, H. Lefebvre-Brion, A. J. Merer, D. A. Ramsay, J. Rostas, and R. N. Zare, J. Mol. Spectrosc. **55**, 500 (1975).
[20] A. G. Maki, G. C. Mellau, S. Klee, M. Winnewisser, and W. Quapp, J. Mol. Spectrosc. **202**, 67 (2000).